ACS Energy LETTERS

http://pubs.acs.org/journal/aelccp

Improving the Energy Efficiency of CO Electrolysis by Controlling Cu Domain Size in Gas Diffusion Electrodes

Joshua A. Rabinowitz, Donald S. Ripatti, Ruperto G. Mariano, and Matthew W. Kanan*

Cite This: *ACS Energy Lett.* 2022, 7, 4098–4105

Read Online

ACCESS | Metrics & More | Article Recommendations | Supporting Information

ABSTRACT: Carbon monoxide electrolysis is a potential bridge between CO_2-to-CO technologies and renewable C_{2+} platform chemicals, but CO reduction (COR) cathode performance must improve to advance these systems. A key challenge is designing COR catalyst layers on gas diffusion electrodes with adequate electron, ion, and gas transport for high current densities. Here we study the effects of Cu domain size and loading in catalyst layers composed of Cu nanoparticles (NPs) and PTFE gas-transporting domains. Using a special ink solvent that stably disperses PTFE, we optimize the PTFE content to create catalyst layers with networks of ∼5 μm wide Cu NP domains. Such layers provide favorable COR transport properties even at very high Cu loadings, which reduces the COR overpotential. In a 24 h electrolysis, an optimized Cu/PTFE electrode achieves a 73.5% single-pass conversion efficiency at 200 mA cm^{-2} and 2.13 V with 76% Faradaic efficiency for COR, including 18% for propanol.

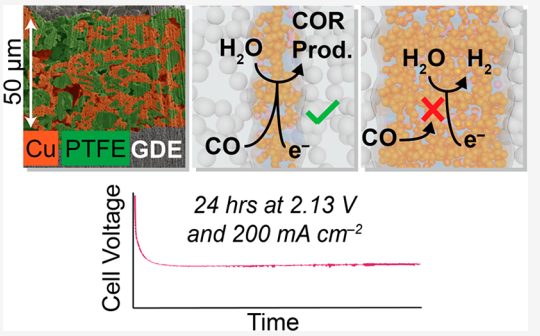

The rapid growth of renewable electricity has greatly increased efforts to develop CO_2 and CO electrolysis for the production of chemicals and fuels that are currently derived from fossil resources. The cathode performance for the CO_2 or CO reduction reactions (CO_2R and COR) is a key determinant of the energy and carbon efficiency of these systems. CO_2R and COR catalyzed by Cu materials are of particular interest because they generate platform C_{2+} products such as ethylene, propanol, ethanol, and acetate.[1−4] The ability to perform these reactions at high current densities while minimizing the overall cell voltage at steady state is essential for advancing electrochemical C_{2+} production toward commercial applications.

Alkaline electrolytes minimize the overpotentials of CO_2R and COR with Cu catalysts because the electrochemical reaction rates depend on the electron driving force but not the proton activity. However, alkaline conditions cannot be maintained at steady state for CO_2R because the thermodynamically favorable and rapid reaction between CO_2 and OH^- to form (bi)carbonate (HCO_3^- and CO_3^{2-}) drives the system to near-neutral pH.[5−7] Both the cathode and anode overpotentials are very high at near-neutral pH, imposing a large voltage penalty on the cell.[8] In addition, a large fraction of the input CO_2 ends up being released at the anode as a mixture with O_2.[9] All reported steady-state cell voltages for CO_2 reduction to C_{2+} products using gas diffusion electrodes (GDEs) exceed 3.5 V at current densities ≥200 mA cm^{-2}.[10−12]

Because CO reacts with OH^- very slowly,[13] alkaline pH can be maintained at steady state in COR, which is beneficial for the cell voltage. A two-step process using a solid oxide electrolyzer to convert CO_2 to CO, followed by COR to generate C_{2+} products, is a promising alternative to direct CO_2R.[14] The electric power consumption of a commercial solid oxide cell operating in tandem with a 2−2.5 V CO electrolysis cell would be substantially lower than that of a direct CO_2 electrolysis cell operating at 3−3.5 V (Figure S1).[15]

While much progress has been made for CO electrolysis in the past several years,[16−21] further improvements in energy efficiency, rate, and selectivity are needed to demonstrate its value for C_{2+} production. One simple approach to decreasing the COR overpotential is to increase the catalytically active Cu surface area. The Cu catalyst in a COR GDE is typically in the form of nanoparticles (NPs). While more intricate nanostructuring can be used to increase the surface area per mass, it

Received: August 31, 2022
Accepted: October 17, 2022
Published: October 25, 2022

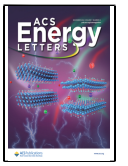

https://doi.org/10.1021/acsenergylett.2c01978
ACS Energy Lett. 2022, 7, 4098−4105

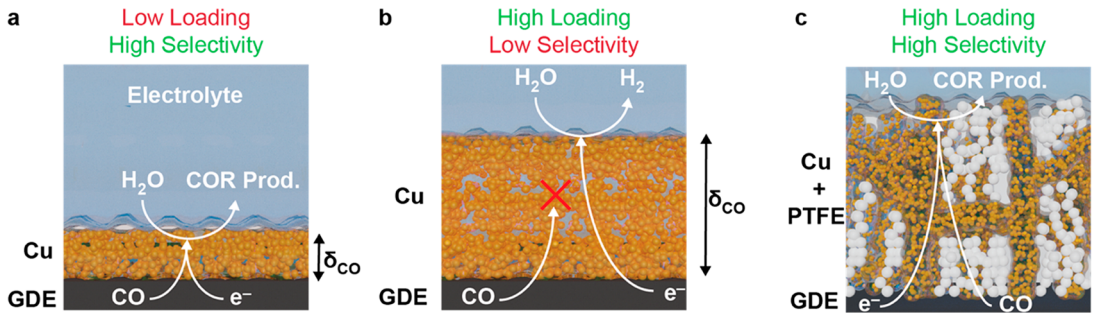

Figure 1. Schematic depictions of the transport of CO and electrons through various catalyst layers containing (a) low Cu loading, (b) high Cu loading, and (c) high Cu loading with gas-transporting PTFE domains.

is difficult to create high-surface-area nanostructures that are stable under GDE electrolysis conditions. It is therefore critical to develop ways to increase the catalyst loading (mass per electrode area) while ideally maintaining the same catalytically active surface area per mass.

Unfortunately, simply loading more catalyst NPs on a GDE can readily increase selectivity for the hydrogen evolution reaction (HER) at the expense of COR or CO_2R.[22] Under the conditions of electrolysis, the Cu NPs in the catalyst layer are wetted with a thin layer of electrolyte or fully submerged in electrolyte (flooded).[23,24] At a low loading, the catalyst layer is thin, so the maximum diffusion length for CO molecules (δ_{CO}) through electrolyte to reach the Cu surfaces distal from the GDE is short (Figure 1a). In this scenario, CO molecules can rapidly diffuse to all Cu surfaces in the catalyst layer to be reduced. At a high loading, however, the catalyst layer is thicker, which increases δ_{CO}. CO must therefore diffuse a longer distance to reach the Cu surfaces farthest away from the GDE. The flux of CO to this region of the catalyst layer is therefore small, which starves it of CO at high current densities and causes it to switch to HER catalysis (Figure 1b). These transport gradients are much steeper in catalyst layers performing COR than CO_2R because CO is ∼30× less soluble in water than CO_2. Polymers with hydrophobic components (such as PTFE or ionomers) can be added to the catalyst layer to improve gas transport and thereby enable the use of a higher catalyst loading for COR or CO_2R.[11,25−31] If the hydrophobic domains are porous and well dispersed, they provide a path for CO transport to the catalyst farthest from the GDE (Figure 1c). In these catalyst layers, the size of the Cu domains dictates δ_{CO} because CO must dissolve in the electrolyte and diffuse from the edge of the hydrophobic domain to the center of the catalyst domain to reach the most distal regions. Therefore, catalyst domain size likely plays a key role in determining COR selectivity in thick catalyst layers.

The catalyst domain sizes can, in principle, be controlled by varying the PTFE content relative to the catalyst NP content in the ink dispersion. However, PTFE does not form a stable dispersion with typical ink solvents, which results in large PTFE agglomerates after deposition[32] and a wide range of catalyst domain sizes. PTFE contents in COR or CO_2R GDE catalyst layers are typically limited to <30 wt%[27,31] unless the ink is stabilized with surfactants or Nafion,[25,26,30] but these additives can reduce the catalyst layer's hydrophobicity.[32] The use of additional ink components such as Nafion also adds complexity to the catalyst layer, making it challenging to isolate the effects of catalyst domain size on transport and overall performance.

Here, we describe a way to control the Cu domain size in GDE catalyst layers by using a solvent mixture to create PTFE dispersions in catalyst inks that are sufficiently stable for spray deposition. By adjusting the PTFE content, we find that catalyst layers with a network of ∼5 μm wide Cu domains surrounded by hydrophobic domains provide sufficient gas, ion, and electron transport to enable high catalyst loadings without sacrificing selectivity. Further decreasing the Cu domain size results in electrically isolated regions of catalyst that increase cathode overpotentials, while larger domains become CO transport limited. With optimized catalyst domain size, the loading of Cu can be increased >10× compared to a Cu-only catalyst layer, which decreases the COR overpotential by 150 mV. At 8 bar CO pressure in a zero-gap cell, a Cu/PTFE electrode produced 18% propanol at an applied current density of 200 mA cm^{-2} and a cell voltage of 2.13 V. This performance was stable over a 24 h electrolysis and is the lowest reported steady-state cell voltage for COR at a current density ≥200 mA cm^{-2}. Our results provide design strategies to optimize the architecture of the GDE catalyst layer for high-performance COR.

Preparation and Characterization of Cu/PTFE Catalyst Layers. To vary the catalyst and hydrophobic domain sizes in GDE catalyst layers over a wide range, we developed an ink that stably disperses PTFE. Isopropanol is commonly used as a solvent for GDE catalyst inks, but at high loadings PTFE NPs rapidly crash out of isopropanol suspensions. For example, PTFE NPs begin to crash out of a freshly prepared 8 mg mL^{-1} suspension in isopropanol in less than 30 s (Figure S2). *tert*-Butyl alcohol (*t*-BuOH) is more hydrophobic than isopropanol, making it a good candidate for forming a stable PTFE suspension. While *t*-BuOH is a solid at room temperature, its freezing point can be depressed by adding isopropanol. We found that sonicating PTFE particles in 1 M isopropanol in *t*-BuOH in an ice bath creates suspensions that are stable for >3 min (Figure S2). It is important to perform the sonication at low temperature to avoid thermal degradation of the PTFE particles. We therefore prepared Cu/PTFE catalyst inks by sonicating Cu NPs and PTFE particles in cold 1 M isopropanol in *t*-BuOH. The inks were used immediately in a custom spray deposition system to deposit catalyst layers on GDE electrodes.

A series of electrodes were prepared in which the catalysts layers contained 33%, 50%, 67%, and 75% PTFE by mass, with Cu NPs making up the mass balance (Cu/PTFE GDEs). Electrode cross sections were prepared using an Ar mill and characterized by scanning electron microscopy (SEM) and energy-dispersive X-ray spectroscopy (EDS). The SEM images were colorized using the EDS images to differentiate the Cu

https://doi.org/10.1021/acsenergylett.2c01978
ACS Energy Lett. 2022, 7, 4098−4105

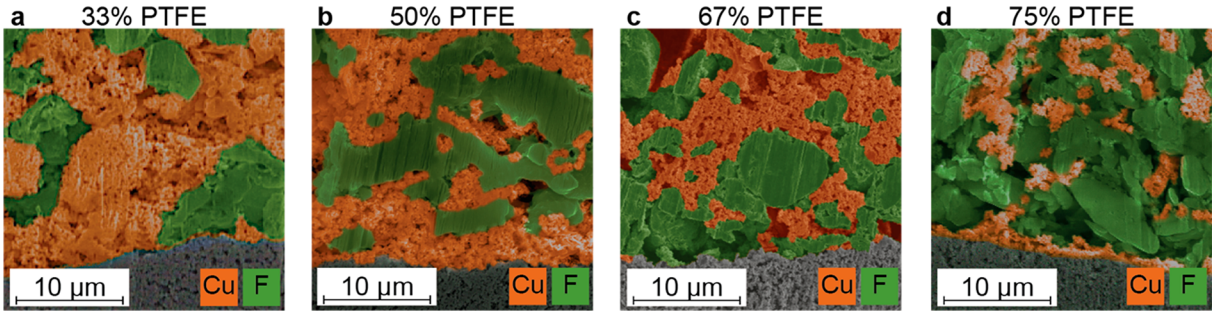

Figure 2. Colorized cross-sectional SEM images of Cu/PTFE GDEs with (a) 33%, (b) 50%, (c) 67%, and (d) 75% PTFE by mass in the catalyst layer.

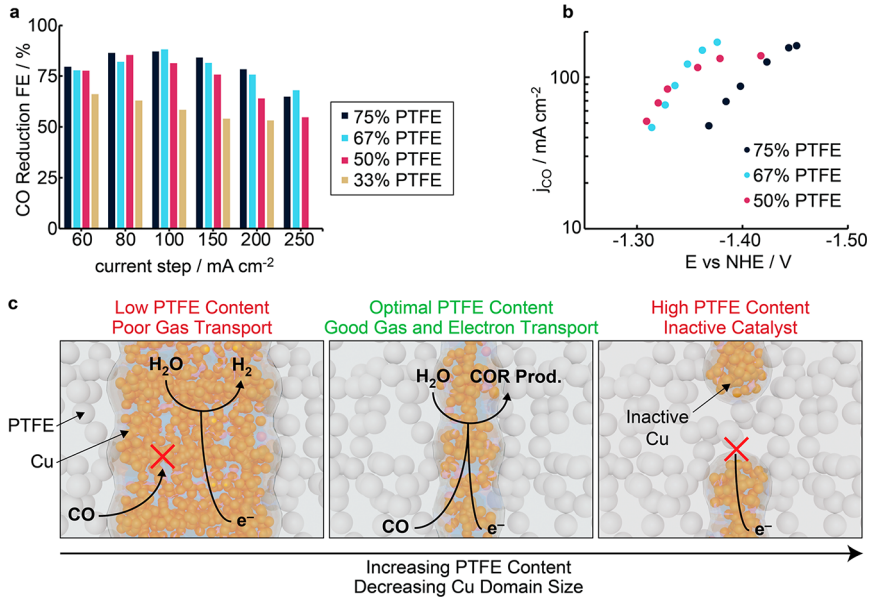

Figure 3. Effect of PTFE content on COR performance. (a) COR FE (all products) vs total current density and (b) COR Tafel plots for Cu/PTFE GDEs containing various PTFE loadings with a fixed Cu loading of 1000 μg cm^{-2}. (c) Schematic representation of CO and electron transport through Cu domains with varying size in Cu/PTFE electrodes.

and PTFE textures (Figures S3–S5). The cross sections reveal that the size of the Cu domains decreases as the PTFE loading is increased (Figures 2 and S3–S6). With 33% PTFE, most of the catalyst domains span 10s of μm. The 50% and 67% PTFE electrodes show a mixture of large (>10 μm) and small (<5 μm) domains, whereas for the 75% PTFE electrode all imaged Cu domains are <5 μm across. The electrodes containing 33–67% PTFE have networks of Cu connected throughout the catalyst layer. While many Cu domains in the 75% PTFE electrode are connected and well dispersed, there are some clusters of Cu that appear to be isolated, which would render them electrochemically inactive. We note that the absence of pores in the observed PTFE domains in Ar-milled samples is likely a result of PTFE melting during Ar milling. Characterization of a Cu/PTFE GDE sectioned using a microtome revealed large pores in the PTFE domains, which are beneficial for gas transport (Figures S7 and S8).

Effects of PTFE Loading on Electrochemical Performance. To assess the effects of Cu domain size on COR performance, the Cu/PTFE GDEs electrodes with varying PTFE content were evaluated in stepped-current electrolysis using our previously reported gas diffusion cell.[17] The Cu loading of each electrode was held constant at ~1000 μg cm^{-2}, and the total geometric current density (j_{tot}) was varied between 60 mA cm^{-2} and 250 mA cm^{-2}. CO was delivered through an interdigitated flow field to the GDE at 1 sccm, and 1 M NaOH was flowed over the front face of the GDE at 150 μL min^{-1}. Humidified N_2 supplied a Nafion membrane electrode assembly (MEA) anode performing water oxidation at the counter electrode (see Figure S9A for electrolysis setup). Cathode potentials were *iR* compensated using impedance spectroscopy (Figure S10).

The electrolysis results demonstrate that PTFE content is critical for optimizing COR performance. At a PTFE loading of 33%, the Faradaic efficiency (FE) for COR (including all products) was 66% at j_{tot} = 60 mA cm^{-2} but declined in favor of H_2 evolution as j_{tot} was increased (Figure 3a). At $j_{tot} \geq 60$ mA cm^{-2}, bubble generation in the catholyte caused noise in the voltage trace (Figure S11). At 50% PTFE, the COR FE reached a peak of 85% at j_{tot} = 80 mA cm^{-2} before decreasing at higher current densities. Full product distributions are shown in Figure S12. Tafel plots of the geometric current density for COR to all products (j_{CO}) vs cathode potential are shown in Figure 3b. For the 33% and 50% PTFE electrodes, the Tafel plots deviate from linearity at j_{CO} > 100 mA cm^{-2}, which implies a CO mass transport limitation in this regime. Increasing the PTFE loading to 67% improved the performance, increasing the COR FE at $j_{tot} \geq 100$ mA cm^{-2} and

https://doi.org/10.1021/acsenergylett.2c01978
ACS Energy Lett. 2022, 7, 4098–4105

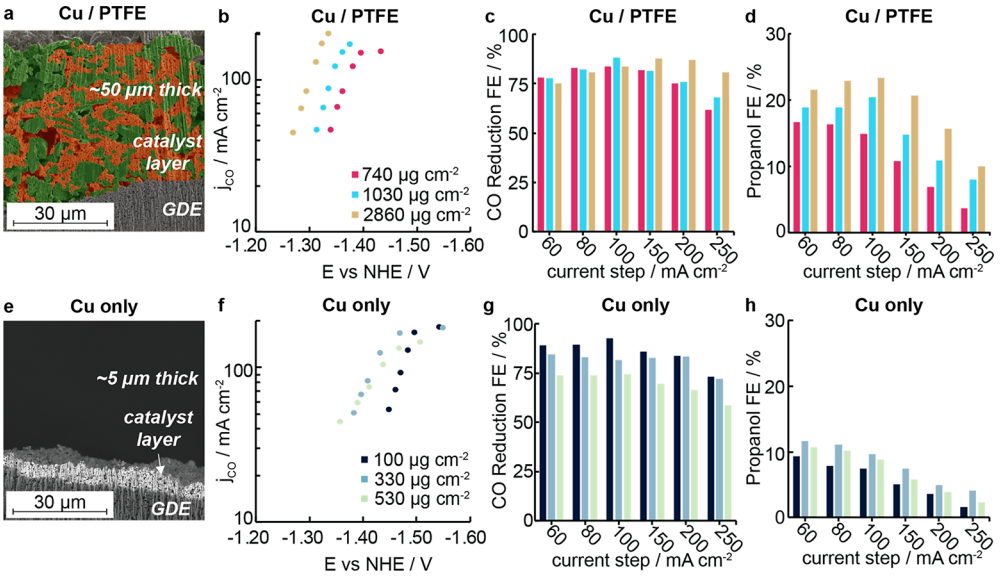

Figure 4. Effect of Cu loading on COR performance. (a) Colorized cross-sectional SEM of a 67% PTFE electrode containing 1400 μg cm^{-2} Cu. (b) COR Tafel plots, (c) COR FE (all products) vs total current density, and (d) propanol FE vs total current density for Cu/PTFE GDEs with 67% PTFE containing various Cu mass loadings. (e) Cross-sectional SEM of a Cu/GDE containing 520 μg cm^{-2} Cu. (f) COR Tafel plot, (g) COR FE, and (h) propanol FE for Cu/GDEs (no PTFE) containing various Cu mass loadings.

extending the linear range of the COR Tafel plot to j_{CO} = 150 mA cm^{-2}. Increasing the PTFE loading to 75% resulted in similar selectivity to 67% PTFE (Figure 3a); however, the Tafel plot shifted to more negative cathode potentials, meaning that this electrode has a larger COR overpotential compared to those with lower PTFE loadings (Figure 3b).

The PTFE dependence of COR performance combined with the cross-sectional electrode images support a model in which the Cu domain size affects CO transport to the catalyst surface and the catalytically active Cu surface area (Figure 3c). At PTFE loadings ≤50%, many of the Cu domains are too large (>10 μm) to allow for effective CO transport into the center of the domains. At high j_{tot}, the inner portions of these domains (distal from the hydrophobic domains) are therefore starved of CO and instead perform HER, which lowers the COR FE. At PTFE ≥ 75%, there are no large Cu domains, but some of the Cu domains are electrically insulated from the GDE (Figure 2d), which lowers the catalytically active Cu surface area and therefore increases the overpotential (see Note S2 for further discussion). A 67% PTFE loading provides small enough Cu domains to allow effective CO transport to all the Cu surfaces while still maintaining electrical connectivity between all the domains (Figure 3c).

Effect of Cu Loading on Electrochemical Performance. We next tested the Cu loading dependence of COR performance using the optimized PTFE content. A series of Cu/PTFE GDEs were prepared with 67% PTFE and various Cu loadings. At fixed PTFE content, increasing the Cu loading corresponds to increasing the catalyst layer thickness. Cross-sectional SEM of an electrode with a Cu loading of 1400 μg cm^{-2} revealed a total catalyst layer thickness of ~50 μm with ~5 μm Cu domains that were well connected throughout the entire layer (Figure 4a). Three electrodes with Cu loadings of 740, 1030, and 2860 μg cm^{-2} were evaluated in stepped current electrolysis under the same conditions described above (Figures 4b–d and S13–S16). An electrode containing 4000 μg cm^{-2} Cu was also prepared, but the catalyst layer was mechanically unstable due to its thickness and cracked during the electrode preparation process. As seen in the COR Tafel plots (Figure 4b), increasing the Cu loading across this series reduces the COR overpotential by ~70 mV. The electrodes show similar COR FE at moderate current densities, reaching 83–88% at j_{tot} = 100 mA cm^{-2} (Figure 4c). At the higher j_{tot} steps, the COR FEs for the 740 and 1030 μg cm^{-2} electrodes decline, whereas the 2860 μg cm^{-2} electrode maintains 87–88% FE at 150 and 200 mA cm^{-2} before declining slightly to 81% at the 250 mA cm^{-2} step. These results demonstrate that adding more Cu with 67% PTFE increases the Cu surface area that is electrochemically active for COR. Thus, even Cu/PTFE GDE catalyst layers that are several 10s of μm thick provide CO transport to all the Cu domains.

The difference in COR FE at high j_{tot} between the highest and lower Cu loading electrodes can be explained by considering the surface area normalized (specific) current densities. The lower loading electrodes experience a higher specific current density, which leads to a larger CO concentration gradient within domains. At high j_{tot}, the interior portions of the Cu domains in the 740 and 1030 μg cm^{-2} electrodes are depleted in CO and start to favor HER, whereas the CO gradients are less pronounced for the 2860 μg cm^{-2} electrode, which allows it to maintain a much higher COR FE. Increased HER activity at high specific current density has been shown in CO_2 reduction studies.[33]

Remarkably, the 2860 μg cm^{-2} electrode operates at 79.1% single-pass CO conversion at j_{tot} = 250 mA cm^{-2} (Table S1). The small drop in COR FE at this current density, and the associated deviation from linearity in the Tafel plot, result from CO depletion because of this high conversion. Increasing the CO flow rate from 1 to 5 sccm boosts the COR FE at 250 mA cm^{-2} (Figure S17). The ability to achieve high single-pass conversion at elevated current density is critical for minimizing the energy demand of product purification.[34]

The Cu loading also affects the selectivity among the various CO reduction products, which are primarily ethylene, propanol, and ethanol. Interestingly, increasing the Cu loading increases the FE for propanol with a commensurate decrease in

https://doi.org/10.1021/acsenergylett.2c01978
ACS Energy Lett. 2022, 7, 4098–4105

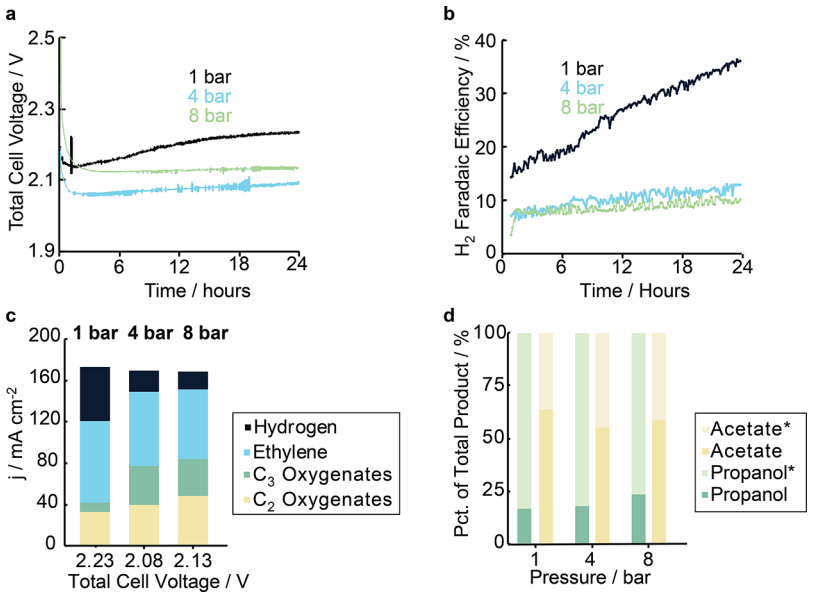

Figure 5. (a) Total cell voltage and (b) H_2 Faradaic efficiency vs time for 24 h electrolysis in a zero-gap cell at 200 mA cm^{-2} at various pressures. The electrolyte was 2 M NaOH, and the CO flow rate was 1 sccm. (c) Net product distributions for the zero-gap cell electrolysis at various pressures vs the average cell potential. 20−35 mA cm^{-2} of current is unaccounted for in these experiments, which is likely due to ethanol produced at the cathode being oxidized to acetate at the anode. (d) Percentage of liquid product crossover from the cathode to the anolyte. Acetate* and propanol* represent the product recovered in the anolyte stream. The electrodes used for these experiments contained 67% PTFE and 2300 μg cm^{-2} Cu.

the FE for ethylene (Figures 4d, S16B, and S18). This result is likely a consequence of the lower cathode overpotential at higher catalyst loading and is consistent with potential-dependent selectivity observed previously for Cu materials.[17,35] Increasing the catalyst surface area by increasing the catalyst loading is a potentially facile route to increase the propanol selectivity and decrease the cathode overpotential.

For comparison, we also evaluated the COR performance of a series of electrodes with no PTFE in the catalyst layer containing 100, 330, and 530 μg cm^{-2} Cu (Cu-only GDEs; see Supporting Information for preparation procedures). The data for these experiments is shown in Figures 4f−h and S19−S21. Increasing the catalyst loading in these Cu-only GDEs incurs selectivity losses and stability issues. For the 100 μg cm^{-2} Cu electrode, the total COR selectivity is 85−93% up to j_{tot} = 200 mA cm^{-2} because the thin catalyst layer at this low loading permits rapid CO transport (Figure 4g). However, methane is produced at j_{tot} > 80 mA cm^{-2} with these electrodes (Figure S21A). Methane is a potent greenhouse gas which would substantially decrease the value of the product stream. Increasing the electrode loading to 330 μg cm^{-2} Cu reduces the CO reduction overpotential by 60−70 mV at low current density (Figure 4f). However, at this loading, the cathode potential is unstable at $j_{tot} \geq$ 200 mA cm^{-2} because of increased H_2 evolution off the front face of the electrode (Figures S20A and S21B). Further increasing the loading to 530 μg cm^{-2} results in COR selectivity losses (Figure 4g,h) and unstable voltage (Figure S20B) at $j_{tot} \geq$ 80 mA cm^{-2}. These results suggest that CO transport is substantially impeded through a catalyst layer containing only 530 μg cm^{-2} Cu, which is only ∼5 μm thick (Figure 4e). Interestingly, the 67% PTFE catalyst layers contain many catalyst domains that are ∼5 μm in diameter, yet they exhibit high COR selectivity. The difference is that CO can approach the center of a domain from multiple sides in a Cu/PTFE catalyst layer, and therefore the diffusion length is shorter than for a Cu-only electrode. These results demonstrate that hydrophobic domains are beneficial for managing the transport of gas, ions, water, and electrons for catalyst layers >5 μm thick.

Evaluation in Zero-Gap Cell. To assess the full cell performance with Cu/PTFE GDEs, we performed experiments using our previously reported zero-gap cell (Figure S9b).[17] In the zero-gap cell, there is no catholyte and the cathode is in direct contact with an ion-transporting membrane, which decreases ion transport resistance in the cell and allows the cathode side to be pressurized with CO. Liquid products generated during electrolysis either diffuse out of the catalyst layer through hydrophilic pores in the GDE and exit the cell through the cathode flow field or are transported across the membrane into the anolyte. Liquid products that are collected off the cathode are more concentrated than those produced in a cell with a flowing catholyte.

Zero-gap cells were assembled using 67% PTFE Cu/PTFE GDEs with ∼2350 μg cm^{-2} Cu loading and a NiFeOH-coated Ti foam anode. Because the GDEs are very hydrophobic, rapid water transport from the anolyte is required to induce cathode wetting. Water transport through an anion-exchange membrane such as Fumasep FAA 3-50 was too sluggish to wet the cathode, resulting in high initial cell voltages (>5 V). Therefore, Nafion 212 was used as the ion-exchange membrane because of its high water permeability. Electrolysis was performed galvanostatically for 24 h at 200 mA cm^{-2} with CO flowing at 1 sccm through the cathode block and 2 M NaOH recirculating through the anode. The data for these experiments are shown in Figures 5 and S22.

At 1 bar CO, the full cell voltage declined for the first few hours but then gradually increased to reach a plateau value of ∼2.23 V (Figure 5a). The FE for H_2 was initially ∼14% but rose to ∼36% by the end of the experiment (Figure 5b). These results suggest that some hydrophobic pores in either the

https://doi.org/10.1021/acsenergylett.2c01978
ACS Energy Lett. 2022, 7, 4098−4105

catalyst layer or the microporous layer of the GDE fill with liquid products over the course of the electrolysis, impeding CO transport to Cu domains (see below).[36] The product distribution averaged over the 24 h experiment is shown in Figures 5c and S22. Ethylene (39% FE) and acetate (16% FE) were the major CO reduction products, along with propanol (4% FE) and small amounts of ethanol and allyl alcohol.

We note that 75−80% of the propanol and 40−45% of the acetate generated in this zero-gap cell are recovered in the anolyte stream due to liquid product transport across the Nafion membrane (Figures 5d and S22−S24). Anodic oxidation of propanol and ethanol results in propionate and additional acetate formation, which accounts for 20−35 mA cm^{-2} of the "missing" current density in Figure 5c (see Note S3 for details). Catalytic oxidation of alcohols on NiFeOH has been previously demonstrated in COR cells.[21] Increasing the thickness of the Nafion membrane resulted in modest reduction of alcohol crossover, but at a ∼200 mV greater cell voltage (Figure S26). Alcohol crossover through ion-exchange membranes is a well-known problem in both the fuel cell and CO_2 electrolysis literature.[21,37−40] Innovations in membrane technology or electrolysis cell design will be necessary to generate concentrated alcohol streams from CO_2 or CO electrolysis.[41−44]

Increasing the CO pressure to 4 bar lowered the average cell voltage to 2.08 V, the lowest cell voltage reported to date for COR at $j_{tot} \geq 200$ mA cm^{-2} (Table S2), and increased the overall selectivity for COR (Figure 5a,c). The higher pressure also changed the COR product distribution such that the FE for propanol increased to 19%. This result demonstrates that the selectivity depends on the CO concentration in the electrolyte wetting the catalyst particles at a fixed CO flow rate. Further increasing the CO pressure to 8 bar did not substantially change the propanol FE but slightly increased the overall liquid product selectivity. At 4 bar, the single-pass conversion was 70%, which increased to 73.5% at 8 bar (Table S3).

Increasing the CO pressure also improves the stability of the electrolysis (Figure 5a,b). At 4 bar CO, the cell voltage increased by only 30 mV over 24 h; the H_2 FE was only 7% initially and increased to 13%. At 8 bar CO, the cell voltage and H_2 FE only increased by 10 mV and ∼2%, respectively. The slower rate of HER increase at elevated pressure is likely because increased CO pressure prevents liquid product permeation into the hydrophobic gas-transporting pores. The cell voltage for the experiment at 8 bar was 2.13 V, ∼50 mV higher than 4 bar, but this difference may be caused by variability in anode performance (Figure S27). These results highlight the voltage, selectivity, and stability benefits from operating a zero-gap cell at elevated CO pressure.

In summary, our results demonstrate the importance of controlling domain sizes in COR catalyst layers containing Cu and hydrophobic components to access layers with high Cu loadings that transport electrons, ions, and CO effectively. The benefits of such catalyst layers include reduced overpotential, voltage stability, high COR vs HER selectivity at high current density and single-pass CO conversion, and no methane formation. Reduced overpotential favors oxygenates, including high-value products such as propanol, but addressing membrane crossover is necessary to make these syntheses viable. Further development of catalyst ink formulations may enable the preparation of layers with even smaller Cu domains and consequently higher active surface area without compromising electrical conductivity, which could further improve COR performance.

■ ASSOCIATED CONTENT

Supporting Information

The Supporting Information is available free of charge at https://pubs.acs.org/doi/10.1021/acsenergylett.2c01978.

Experimental details; comparative electric power consumption analysis; additional SEM and scanning confocal microscope characterization Cu/PTFE GDEs; electrochemical cell schematics; impedance spectra, voltage traces, and full product distributions for data collected in three-electrode cells; additional zero-gap cell experimental data; and single-pass CO conversions for various experiments, including Figures S1−S27, Tables S1−S3, and Notes S1−S3 (PDF)

■ AUTHOR INFORMATION

Corresponding Author

Matthew W. Kanan − *Department of Chemistry, Stanford University, Stanford, California 94305, United States;* orcid.org/0000-0002-5932-6289; Email: mkanan@stanford.edu

Authors

Joshua A. Rabinowitz − *Department of Chemistry, Stanford University, Stanford, California 94305, United States;* orcid.org/0000-0001-9330-0464

Donald S. Ripatti − *Department of Chemistry, Stanford University, Stanford, California 94305, United States*

Ruperto G. Mariano − *Department of Chemistry, Stanford University, Stanford, California 94305, United States*

Complete contact information is available at: https://pubs.acs.org/10.1021/acsenergylett.2c01978

Author Contributions

M.W.K. and D.S.R. conceived the project. J.A.R. designed and performed the experiments and the electrode characterization. R.G.M. performed the electrode characterization of the microtomed electrode. J.A.R. and M.W.K. wrote the initial draft of the manuscript. All authors contributed to editing and revising the manuscript.

Notes

The authors declare the following competing financial interest(s): The authors have filed a patent application based on the electrodes described in this work.

■ ACKNOWLEDGMENTS

We thank the NSF (CHE-1855950) and NASA (80NSSC19M0034) for support of this research. J.A.R. gratefully acknowledges a Stanford Graduate Fellowship. We thank John Perrino for assistance microtoming the gas diffusion electrodes. Part of this work was performed at the Stanford Nano Shared Facilities (SNSF), which is supported by the NSF under award ECCS-2026822.

■ REFERENCES

(1) Hori, Y.; Murata, A.; Takahashi, R.; Suzuki, S. Electroreduction of Carbon Monoxide to Methane and Ethylene at a Copper Electrode in Aqueous Solutions at Ambient Temperature and Pressure. *J. Am. Chem. Soc.* **1987**, *109* (16), 5022−5023.

(2) Hori, Y.; Takahashi, R.; Yoshinami, Y.; Murata, A. Electrochemical Reduction of CO at a Copper Electrode. *J. Phys. Chem. B* **1997**, *101* (36), 7075−7081.
(3) Hori, Y.; Takahashi, I.; Koga, O.; Hoshi, N. Selective Formation of C_2 Compounds from Electrochemical Reduction of CO_2 at a Series of Copper Single Crystal Electrodes. *J. Phys. Chem. B* **2002**, *106* (1), 15−17.
(4) Li, C. W.; Ciston, J.; Kanan, M. W. Electroreduction of Carbon Monoxide to Liquid Fuel on Oxide-Derived Nanocrystalline Copper. *Nature* **2014**, *508* (7497), 504−507.
(5) Ma, M.; Clark, E. L.; Therkildsen, K. T.; Dalsgaard, S.; Chorkendorff, I.; Seger, B. Insights into the Carbon Balance for CO_2 Electroreduction on Cu Using Gas Diffusion Electrode Reactor Designs. *Energy Environ. Sci.* **2020**, *13* (3), 977−985.
(6) Ma, M.; Kim, S.; Chorkendorff, I.; Seger, B. Role of Ion-Selective Membranes in the Carbon Balance for CO_2 Electroreduction via Gas Diffusion Electrode Reactor Designs. *Chem. Sci.* **2020**, *11* (33), 8854−8861.
(7) Larrazábal, G. O.; Strøm-Hansen, P.; Heli, J. P.; Zeiter, K.; Therkildsen, K. T.; Chorkendorff, I.; Seger, B. Analysis of Mass Flows and Membrane Cross-over in CO_2 Reduction at High Current Densities in an MEA-Type Electrolyzer. *ACS Appl. Mater. Interfaces* **2019**, *11* (44), 41281−41288.
(8) Rabinowitz, J. A.; Kanan, M. W. The Future of Low-Temperature Carbon Dioxide Electrolysis Depends on Solving One Basic Problem. *Nat. Commun.* **2020**, *11* (1), 5231.
(9) Kaczur, J. J.; Yang, H.; Liu, Z.; Sajjad, S. D.; Masel, R. I. Carbon Dioxide and Water Electrolysis Using New Alkaline Stable Anion Membranes. *Front. Chem.* **2018**, *6*, 263.
(10) Gabardo, C. M.; O'Brien, C. P.; Edwards, J. P.; McCallum, C.; Xu, Y.; Dinh, C.-T.; Li, J.; Sargent, E. H.; Sinton, D. Continuous Carbon Dioxide Electroreduction to Concentrated Multi-Carbon Products Using a Membrane Electrode Assembly. *Joule* **2019**, *3* (11), 2777−2791.
(11) García de Arquer, F. P.; Dinh, C.-T.; Ozden, A.; Wicks, J.; McCallum, C.; Kirmani, A. R.; Nam, D.-H.; Gabardo, C.; Seifitokaldani, A.; Wang, X.; et al. CO_2 Electrolysis to Multicarbon Prodcts at Activities Greater than 1 A Cm^{-2}. *Science* **2020**, *367* (6478), 661−666.
(12) Huang, J. E.; Li, F.; Ozden, A.; Sedighian Rasouli, A.; Garcia de Arquer, F. P.; Liu, S.; Zhang, S.; Luo, M.; Wang, X.; Lum, Y.; Xu, Y.; Bertens, K.; Miao, R. K.; Dinh, C.-T.; Sinton, D.; Sargent, E. H.; et al. CO_2 Electrolysis to Multicarbon Products in Strong Acid. *Science* **2021**, *372* (6546), 1074−1078.
(13) Patwardhan, A. V.; Sharma, M. M. Kinetics of Absorption of Carbon Monoxide in Aqueous Solutions of Sodium Hydroxide and Aqueous Calcium Hydroxide Slurries. *Ind. Eng. Chem. Res.* **1989**, *28* (1), 5−9.
(14) Jouny, M.; Hutchings, G. S.; Jiao, F. Carbon Monoxide Electroreduction as an Emerging Platform for Carbon Utilization. *Nat. Catal. 2019 212* **2019**, *2* (12), 1062−1070.
(15) Sisler, J.; Khan, S.; Ip, A. H.; Schreiber, M. W.; Jaffer, S. A.; Bobicki, E. R.; Dinh, C. T.; Sargent, E. H. Ethylene Electrosynthesis: A Comparative Techno-Economic Analysis of Alkaline vs Membrane Electrode Assembly vs CO_2-CO-C_2H_4 Tandems. *ACS Energy Lett.* **2021**, *6* (3), 997−1002.
(16) Zhu, P.; Xia, C.; Liu, C.-Y.; Jiang, K.; Gao, G.; Zhang, X.; Xia, Y.; Lei, Y.; Alshareef, H. N.; Senftle, T. P.; Wang, H. Direct and Continuous Generation of Pure Acetic Acid Solutions via Electrocatalytic Carbon Monoxide Reduction. *Proc. Natl. Acad. Sci. U. S. A.* **2021**, *118* (2), e2010868118.
(17) Ripatti, D. S.; Veltman, T. R.; Kanan, M. W. Carbon Monoxide Gas Diffusion Electrolysis That Produces Concentrated C_2 Products with High Single-Pass Conversion. *Joule* **2019**, *3* (1), 240−256.
(18) Wang, X.; Ou, P.; Ozden, A.; Hung, S.-F.; Tam, J.; Gabardo, C. M.; Howe, J. Y.; Sisler, J.; Bertens, K.; Pelayo Garcamp, F.; et al. Efficient Electrosynthesis of N-Propanol from Carbon Monoxide Using a Ag−Ru−Cu Catalyst. *Nat. Energy 2022* **2022**, *7*, 170−176.
(19) Duong, H. P.; Tran, N.-H.; Rousse, G.; Zanna, S.; Schreiber, M. W.; Fontecave, M. Highly Selective Copper-Based Catalysts for Electrochemical Conversion of Carbon Monoxide to Ethylene Using a Gas-Fed Flow Electrolyzer. *ACS Catal.* **2022**, *12*, 10285−10293.
(20) Ji, Y.; Chen, Z.; Wei, R.; Yang, C.; Wang, Y.; Xu, J.; Zhang, H.; Guan, A.; Chen, J.; Sham, T. K.; et al. Selective CO-to-Acetate Electroreduction via Intermediate Adsorption Tuning on Ordered Cu−Pd Sites. *Nat. Catal. 2022 54* **2022**, *5* (4), 251−258.
(21) Overa, S.; Crandall, B. S.; Shrimant, B.; Tian, D.; Ko, B. H.; Shin, H.; Bae, C.; Jiao, F. Enhancing Acetate Selectivity by Coupling Anodic Oxidation to Carbon Monoxide Electroreduction. *Nat. Catal. 2022 58* **2022**, *5* (8), 738−745.
(22) Möller, T.; Ngo Thanh, T.; Wang, X.; Ju, W.; Jovanov, Z.; Strasser, P. The Product Selectivity Zones in Gas Diffusion Electrodes during the Electrocatalytic Reduction of CO_2. *Energy Environ. Sci.* **2021**, *14* (11), 5995−6006.
(23) Weng, L.-C.; Bell, A. T.; Weber, A. Z. Modeling Gas-Diffusion Electrodes for CO_2 Reduction. *Phys. Chem. Chem. Phys.* **2018**, *20*, 16973.
(24) Giner, J.; Hunter, C. The Mechanism of Operation of the Teflon-Bonded Gas Diffusion Electrode: A Mathematical Model. *J. Electrochem. Soc.* **1969**, *116* (8), 1124−1129.
(25) Xing, Z.; Hu, X.; Feng, X. Tuning the Microenvironment in Gas-Diffusion Electrodes Enables High-Rate CO_2 Electrolysis to Formate. *ACS Energy Lett.* **2021**, *6* (5), 1694−1702.
(26) Xing, Z.; Hu, L.; Ripatti, D. S.; Hu, X.; Feng, X. Enhancing Carbon Dioxide Gas-Diffusion Electrolysis by Creating a Hydrophobic Catalyst Microenvironment. *Nat. Commun.* **2021**, *12* (1), 136.
(27) Wang, Q.; Dong, H.; Yu, H.; Yu, H. Enhanced Performance of Gas Diffusion Electrode for Electrochemical Reduction of Carbon Dioxide to Formate by Adding Polytetrafluoroethylene into Catalyst Layer. *J. Power Sources* **2015**, *279*, 1−5.
(28) Li, J.; Chen, G.; Zhu, Y.; Liang, Z.; Pei, A.; Wu, C. L.; Wang, H.; Lee, H. R.; Liu, K.; Chu, S.; et al. Efficient Electrocatalytic CO_2 Reduction on a Three-Phase Interface. *Nat. Catal.* **2018**, *1* (8), 592−600.
(29) Mariano, R. G.; Wahab, O. J.; Rabinowitz, J. A.; Oppenheim, J.; Chen, T.; Unwin, P. R.; Dincă, M. Thousand-Fold Increase in O_2 Electroreduction Rates with Conductive MOFs. *ACS Cent. Sci.* **2022**, *8* (7), 975−982.
(30) Sheng, X.; Ge, W.; Jiang, H.; Li, C. Engineering the Ni-N-C Catalyst Microenvironment Enabling CO_2 Electroreduction with Nearly 100% CO Selectivity in Acid. *Adv. Mater.* **2022**, *34*, 2201295.
(31) Reyes, A.; Jansonius, R. P.; Mowbray, B. A. W.; Cao, Y.; Wheeler, D. G.; Chau, J.; Dvorak, D. J.; Berlinguette, C. P. Managing Hydration at the Cathode Enables Efficient CO_2 Electrolysis at Commercially Relevant Current Densities. *ACS Energy Lett.* **2020**, *5* (5), 1612−1618.
(32) Mao, Q.; Sun, G.; Wang, S.; Sun, H.; Tian, Y.; Tian, J.; Xin, Q. Application of Hyperdispersant to the Cathode Diffusion Layer for Direct Methanol Fuel Cell. *J. Power Sources* **2008**, *175* (2), 826−832.
(33) Lamaison, S.; Wakerley, D.; Kracke, F.; Moore, T.; Zhou, L.; Lee, D. U.; Wang, L.; Hubert, M. A.; Aviles Acosta, J. E.; Gregoire, J. M.; et al. Designing a Zn−Ag Catalyst Matrix and Electrolyzer System for CO_2 Conversion to CO and Beyond. *Adv. Mater.* **2022**, *34* (1), 2103963.
(34) Greenblatt, J. B.; Miller, D. J.; Ager, J. W.; Houle, F. A.; Sharp, I. D. The Technical and Energetic Challenges of Separating (Photo)Electrochemical Carbon Dioxide Reduction Products. *Joule* **2018**, *2* (3), 381−420.
(35) Jouny, M.; Luc, W.; Jiao, F. High-Rate Electroreduction of Carbon Monoxide to Multi-Carbon Products. *Nat. Catal.* **2018**, *1* (10), 748−755.
(36) Leonard, M. E.; Orella, M. J.; Aiello, N.; Román-Leshkov, Y.; Forner-Cuenca, A.; Brushett, F. R. Flooded by Success: On the Role of Electrode Wettability in CO_2 Electrolyzers That Generate Liquid Products. *J. Electrochem. Soc.* **2020**, *167* (12), 124521.
(37) Zhang, J.; Luo, W.; Züttel, A. Crossover of Liquid Products from Electrochemical CO_2 Reduction through Gas Diffusion

https://doi.org/10.1021/acsenergylett.2c01978
ACS Energy Lett. 2022, 7, 4098−4105

Electrode and Anion Exchange Membrane. *J. Catal.* **2020**, *385*, 140−145.
(38) Salvatore, D. A.; Gabardo, C. M.; Reyes, A.; O'Brien, C. P.; Holdcroft, S.; Pintauro, P.; Bahar, B.; Hickner, M.; Bae, C.; Sinton, D.; et al. Designing Anion Exchange Membranes for CO_2 Electrolysers. *Nat. Energy 2021 64* **2021**, *6* (4), 339−348.
(39) Li, Y. C.; Yan, Z.; Hitt, J.; Wycisk, R.; Pintauro, P. N.; Mallouk, T. E.; et al. Bipolar Membranes Inhibit Product Crossover in CO_2 Electrolysis Cells. *Adv. Sustain. Syst.* **2018**, *2* (4), 1700187.
(40) Verbrugge, M. W. Methanol Diffusion in Perfluorinated Ion-Exchange Membranes. *J. Electrochem. Soc.* **1989**, *136* (417), 417−423.
(41) Miao, R. K.; Xu, Y.; Ozden, A.; Robb, A.; O'Brien, C. P.; Gabardo, C. M.; Lee, G.; Edwards, J. P.; Huang, J. E.; Fan, M.; et al. Electroosmotic Flow Steers Neutral Products and Enables Concentrated Ethanol Electroproduction from CO_2. *Joule* **2021**, *5* (10), 2742−2753.
(42) McCallum, C.; Gabardo, C. M.; O'Brien, C. P.; Edwards, J. P.; Wicks, J.; Xu, Y.; Sargent, E. H.; Sinton, D. Reducing the Crossover of Carbonate and Liquid Products during Carbon Dioxide Electroreduction. *Cell Reports Phys. Sci.* **2021**, *2* (8), 100522.
(43) Xia, C.; Zhu, P.; Jiang, Q.; Pan, Y.; Liang, W.; Stavitski, E.; Alshareef, H. N.; Wang, H. Continuous Production of Pure Liquid Fuel Solutions via Electrocatalytic CO_2 Reduction Using Solid-Electrolyte Devices. *Nat. Energy* **2019**, *4* (9), 776−785.
(44) Robb, A.; Ozden, A.; Miao, R. K.; O'Brien, C. P.; Xu, Y.; Gabardo, C. M.; Wang, X.; Zhao, N.; García de Arquer, F. P.; Sargent, E. H.; et al. Concentrated Ethanol Electrosynthesis from CO_2 via a Porous Hydrophobic Adlayer. *ACS Appl. Mater. Interfaces* **2022**, *14* (3), 4155−4162.

https://doi.org/10.1021/acsenergylett.2c01978
ACS Energy Lett. 2022, 7, 4098−4105